ISSN 1330-3651 (Print), ISSN 1848-6339 (Online)
https://doi.org/10.17559/TV-20230103000078
Original scientific paper

Multi-Response Optimization of the Flat Burnishing Process with a High-Stiffness Tool in terms of Surface Characteristics

An-Le VAN, Xuan-Ba DANG*, Trung-Thanh NGUYEN

Abstract: In this work, the surface roughness (*SR*), surface hardness (*SH*), and the thickness of the affected layer (*TL*) of the multi-roller flat burnishing process are optimized.The parameter inputs are the tool rotational speed (*S*), burnishing depth (*D*), and feed rate (*f*). The flat burnishing tool having three rollers was utilized to facilitate burnishing trials. The Kriging models of performances are proposed regarding inputs.The CRITIC method and Crow Search Algorithm (CSA) were employed to select weights and optimality. The optimizing outcomes indicated that the optimal values of the *S*, *f*, and *D* were 912 rpm, 150 mm/min, and 0.12 mm, respectively. The improvements in the *SR*, *SH*, and *TL* were 33.3%, 26.9%, and 48.6%, respectively. The *SR* was primarily influenced by the *f*, followed by the *D* and *S*, respectively. The *SH* and *TL* were primarily influenced by the *D*, followed by the *S* and *f*, respectively. The optimal data could be applied to the practical multi-roller burnishing process to improve surface properties for flat surfaces. The Kriging models and CSA could be efficiently utilized to solve complex issues for burnishing operations and other machining processes.

Keywords: affected layer; hardness; kriging model; multi-roller flat burnishing; roughness

1 INTRODUCTION

The burnishing process is widely applied to enhance surface properties of different components with ferrous and non-ferrous materials. The primary benefits of the burnishing process are low roughness, high hardness, increased compressive stress, and enhanced resistance. Therefore, the optimal conditions of the burnishing process should be selected to increase its applicability.

Different burnishing processes have been optimized to improve performance measures. The ANFIS was applied to develop the surface roughness (*SR*) and surface hardness (*SH*) in terms of the tool rotational speed (*S*), feed rate (*f*), the number of passes (*NP*), and the burnishing force (*BF*) for the ball-burnished Al 7075 T6 [1]. The results indicated that higher values of the *BF* and *NP* could be utilized to enhance the *SR* and *SH*. The artificial neural network (ANN) was employed to forecast the *SR* regarding the *S*, *NP*, *f,* and burnishing depth (*D*) [2]. The results indicated that the deviation between the predictive and actual values was lower than 1%.

The Taguchi method was applied to find optimal *S*, *f*, *NP*, and *BF* for enhancing the *SR* and *SH* of the ball-burnished Ti-6Al-4V [3]. The authors revealed that the enhancements in the *SR* and *SH* were 24.0% and 86.0%. A new ball-burnishing tool was developed to investigate the barrier properties of wood specimens [4]. The authors stated that the water absorption was significantly decreased, while the density and hardness of the surface layer were effectively increased. The response surface methodology (RSM) was applied and optimized the *SR* and *SH* in terms of the *BF*, *f*, *NP*, and width (*W*) [5]. The authors stated that the improvements in the *SR* and *SH* were 95.0% and 12.0%, respectively. The *SR* model of the roller-burnished AA 6061 was developed regarding the *S*, *f*, *NP*, and interference [6]. The results revealed that interference and *f* were the most significant factors. The *SR*, ovality, and bore size models of the burnished cast iron were proposed regarding the *S*, *f*, and penetration allowances, respectively [7]. The optimal values of the *S*, *f*, and penetration allowances were 1100 rpm, 0.11 mm/rev, and 0.03 mm, respectively. The *SR* and *SH* models were developed for the burnished TA2 alloy in terms of the *S*, *f*, and *D* [8]. The authors stated that the *S* and *D* were significant parameters. Shankar et al. indicated that the minimum *SR* and maximum *SH* of the burnished composite were obtained at the dry condition, coated roller, and the *NP* of 3 [9]. The *SR*, *SH*, and *TL* models were proposed in terms of the *S*, *f*, and *D* for the burnished carbon steel, while the optimal values *SR*, *SH*, and *TL* were 0.071 μm, 52.0 HRC, and 131.0 μm respectively [10]. Cagan et al. indicated that the function fitting ANN could be applied to precisely predict the *SR* and *SH* for the ball-burnished magnesium alloy [11]. Nguyen revealed that the *SR*, cylindricity (*CL*), circularity (*CC*), and dimensional deviation of the burnished hole were decreased by 54.4%, 80.2%, 2.1%, and 48.0%, respectively at the optimal values of the *S*, *f*, and *D* [12].

Nguyen and Le emphasized that the enhancements in the energy efficiency, *SR*, and machining noise were 6.9%, 25.0%, and 2.2%, respectively for the burnished SCr440 steel [13]. Nguyen et al. indicated that the maximum roughness was decreased by 17.0% and the Vickers hardness was enhanced by 14.0%, respectively using the optimal operating parameters of the minimum quantity lubrication (MQL) system [14]. Nguyen et al. stated that the energy consumption (*EC*), mean roughness (*MR*), and *CC* were decreased by 12.2%, 14.2%, and 42.5%, respectively with the support of the *S*, *D*, flow rate (*F*), and inlet pressure (*P*) [15]. Prasad and John emphasized that the *SR* of 0.1506 μm, the *SH* of 57.9 HV, and the *CC* of 0.015 mm of the external surface could be obtained with the aid of the RSM [16]. Van and Nguyen presented that the CYL and CIC of the burnished hole were decreased by 53.1% and 57.8 %, respectively, at the optimal point of the spray nozzle (*DS*), the spray elevation angle (*A*), flow rate (*F*), and air pressure (*P*) [17]. The impacts of the *S*, *NP*, *f*, and *BF* on the *SH* and residual stress for the diamond burnishing of the structural steel were analyzed by Varga and Ferencsik [18]. The authors stated that a low *S* could be applied to produce the desired changes. The ANFIS and genetic algorithm were applied to find MQL parameters for decreasing the *EC* and particulate matter index (*PI*) of the internal burnishing process [19]. The authors stated that the *EC* and *PI* were decreased by 8.0% and 15.7%, respectively. Branko Tadic et al. revealed that a high-stiffness tool enables better workpiece dimensional and

geometrical accuracies [20]. The reduction factors in the *CL* and *CC* were 2.28 and 1.81, respectively. The *SR* model of the ball burnishing based on milling kinematics was used to evaluate the functionality of a designed tool [21]. The authors presented that a higher *D* increased the internal stress and decreased the surface roughness. Tadic et al. proposed the *SR* model of the burnished EN AW-6082 using a high-stiffness tool regarding the *BF*, *f*, and *NP* [22]. The result indicated that the *SR* value was equivalent to polishing. The ultrasonic vibration-assisted ball burnishing tool was developed to improve the surface properties of the burnished Ti-6Al-4V [23]. The results indicated that the improvements in the *SR*, *MR*, and *SH* were 61.6%, 66.1%, and 39.5%, respectively. Kanovic et al. emphasized that the ANN and support vector regression provided high accuracy to predict the *SR* value of the burnished AISI 4130 [24]. However, the drawbacks of the aforementioned works can be expressed as:

The *TL* model for the multi-roller flat burnishing process has not been presented.

The optimal parameters have not been selected for enhancements in the *SR*, *SH*, and *TL*.

It is necessary to develop an optimization approach to reduce experimental costs and find global results.

2 OPTIMIZATION APPROACH

The optimizing approach is expressed in Fig. 1:

Step 1: Computing experimental data [25, 26].

The *SR* value is computed as:

$$SR = \frac{\sum_{i=1}^{n} Ra_i}{n} \tag{1}$$

where, Ra_i denotes the average roughness at the *i*-th measured point.

The *SH* value is calculated as:

$$SH = \frac{\sum_{i=1}^{n} BH_i}{n} \tag{2}$$

where, BH_i denotes the Brinell hardness at the *i*-th measured location.

The *TL* value is calculated as:

$$TL = \frac{\sum_{i=1}^{n} TL_i}{n} \tag{3}$$

where, TL_i denotes the measured thickness at the *i*-th measured location.

Step 2: Developing Kriging models of the responses.

The Kriging surrogate model is expressed as:

$$y(x) = \beta f(x)^T + Z(x) \tag{4}$$

where, x, $\beta f(x)^T$, and $Z(x)$ are design variables, regression term, and random deviation, respectively. The covariance of $Z(x)$ between two points x_a and x_b is expressed as:

$$\operatorname{cov}\left(Z(x_a),\ Z(x_b)\right) = \sigma_R^2 R\left(x_a, x_b\right) \tag{5}$$

where, σ^2_Z and $R(x_a, x_b)$ are the variance and correlation function, respectively.

The correlation function is expressed as:

$$R\left(x_a,\ x_b\right) = \exp\left[-\sum_{i=1}^{d} \theta_i \left(x_{ai} - x_{bi}\right)^2\right] \tag{6}$$

where, d and θ_i are the dimension of the design variables and undetermined parameter, respectively.

The regression parameter β is expressed as:

$$\beta = \left(X^T R^{-1} X\right)^{-1} \left(X^T R^{-1} Y\right) \tag{7}$$

The predictive Kriging model is expressed as:

$$\hat{y}\left(x^*\right) = f\left(x^*\right)\beta + r\left(x^*\right)^T R^{-1}\left(Y - X\beta\right) \tag{8}$$

where, the vector $r(x^*)^T = [R(x^*, x_1), \ldots, R(x^*, x_N)]$.

The deviation between experiments and predictive models is computed as:

$$ER = \frac{ya - yp}{ya} \tag{9}$$

where, y_a and y_p are the actual and predictive values, respectively.

Step 3: Determination of the weight of each response using the CRITIC method.

The normalized response (x_{ij}) is computed as:

$$x_{ij} = \frac{x_{ij} - x_j^{word}}{x_j^{best} - x_j^{word}} \tag{10}$$

The standard deviation (s_j) is calculated as:

$$s_j = \sqrt{\frac{\left(\sum_{i=1}^{m} x_{ij} - x_m\right)^2}{m-1}} \tag{11}$$

Computation of the measure of the conflict (I_j):

$$I_j = \sum_{k=1}^{m} (1 - r_{jk}) \tag{12}$$

Determination of the symmetric matrix of $n \times n$ with element r_{jk}, which is a linear correlation coefficient between the vectors x_j and x_k.

Determination of the quantity of the information (C_j):

$$C_j = s_j \sum_{k=1}^{m} (1 - r_{jk}) \tag{13}$$

The computed weight (ω_i) is calculated as:

$$\omega_i = \frac{C_j}{\sum_{k=1}^{n} C_j} \tag{14}$$

Step 4: The optimal data are selected using the CSA. The operation steps of the CSA are expressed in Fig. 2:

- Setting initial parameters of the CSA, including the population size (p), iteration number (t), flight step size (fz), and awareness probability (ap).
- Generation of individual crows and memory matrix.
- Evaluation of the fitness of each crow.
- Production of a new location for each crow.
- Evaluation of the fitness of each crow at a new position.
- Updating the memory matrix of each crow.

The optimizing inputs and their levels, including the S, f, and D are shown in Tab. 1. The levels of the S and f are selected based on the characteristics of the machine tool. The levels of the D are determined according to the configuration of the burnishing tool. Consequently, the optimizing issue is expressed as:

Minimize the SR; Maximize the SH and TL;

Constraints: $400 \leq S \leq 12000$ rpm; $100 \leq f \leq 500$ mm/min; $0.04 \leq D \leq 0.12$ mm.

Table 1 Optimizing parameters of the multi-roller flat burnishing process

Symbol	Parameters	Values
S	Tool rotational speed / rpm	500-900-1300
f	Feed rate / mm/min	150-3500-550
D	Burnishing depth / mm	0.06-0.09-0.12

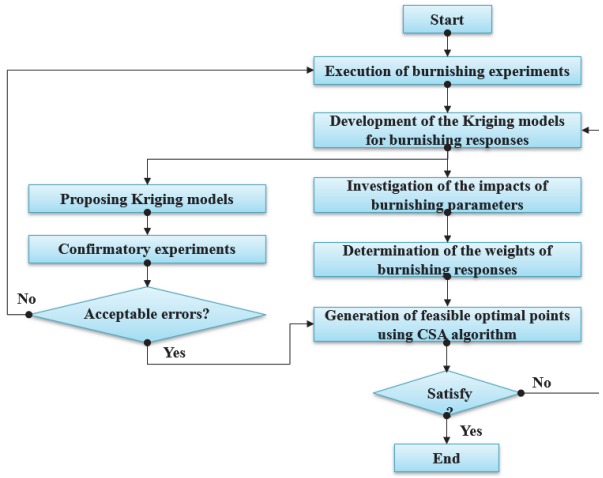

Figure 1 The schematic illustration of the external burnishing operation

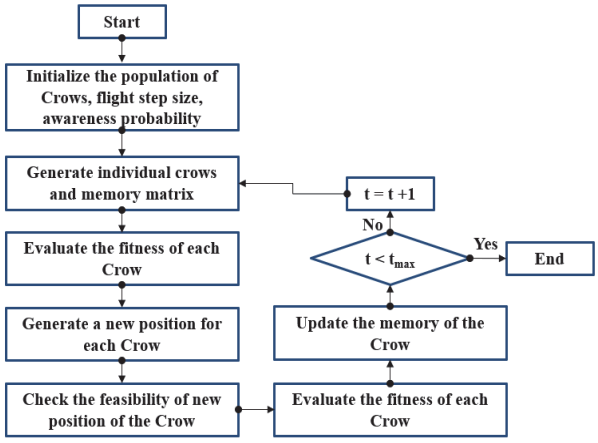

Figure 2 The operation steps of the CSA

3 EXPERIMENTAL SETTING

Burnishing experiments are conducted using a CNC milling machine, in which the specimen is tightly clamped using the precision vise (Fig. 3). The flood condition using the water-based oil entitled EMCOOL E-960V is utilized. The AISI 5150 steel is utilized due to its applications in the marine and automotive industries. The rectangular bar has a length of 70 mm, a width of 20 mm, and a height of 10 mm. The chemical compositions of the chosen material are shown in Tab. 2.

The Ernst hardness tester is applied to capture the Brinell hardness on the burnished surface.The pressed load of 150 kf and dwell time of 5 seconds are used for all hardness tests. The resolution of 0.1 Brinell is applied to capture the experimental data. The average hardness is computed from three locations of similarity. A Mitutoyo SJ-301 using a probe head is employed to measure the roughness, in which a measured length of 4 mm is employed. The measured range of 0.05 - 40 mm and the resolution of 0.01 µm are employed to enhance accuracy. The average roughness is computed from three locations of similarity. The electron microscope AXIO A2M is used to explore the thickness of the depth of the affected layer. The magnifications are 50, 100, 200, and 500, respectively. The average thickness is computed from five locations of similarity. The example values of burnishing responses are presented in Fig. 4.

Table 2 Chemical compositions of AISI 5150 alloy steel

Element	Mn	Cr	C	Si	S	P	Fe
%	0.80	0.80	0.52	0.20	0.04	0.035	balance

Table 3 Experimental data for the multi-roller flat burnishing process

No.	S / rpm	F / mm/min	D / mm	SR / µm	SH / HB	TL / µm
Training data for Kriging models						
1	900	350	0.09	0.26	390	99.8
2	500	350	0.06	0.35	335	51.3
3	1300	350	0.06	0.49	413	91.2
4	500	350	0.12	0.26	405	95.3
5	900	350	0.09	0.27	391	98.5
6	1300	350	0.12	0.41	524	136.4
7	900	150	0.06	0.26	393	102.3
8	900	550	0.06	0.43	300	78.9
9	900	350	0.09	0.26	387	99.4
10	900	150	0.12	0.18	495	145.9
11	900	550	0.12	0.34	382	124.5
12	500	150	0.09	0.26	381	93.2
13	900	350	0.09	0.27	392	98.8
14	500	550	0.09	0.43	292	65.4
15	1300	150	0.09	0.41	493	127.6
16	1300	550	0.09	0.57	377	111.4
17	900	350	0.09	0.26	391	98.4
Testing data for Kriging models						
18	600	250	0.06	0.29	356	69.8
19	800	450	0.08	0.32	338	82.8
20	900	400	0.1	0.27	393	104.7
21	1200	350	0.11	0.35	477	125.4
22	950	200	0.06	0.28	393	97.1
23	1050	300	0.08	0.31	408	101.3
24	850	250	0.12	0.18	470	130.6

Table 4 The values of Kriging model parameters

Responses	Correlation parameter θ_i			Scalar factor β
	V	f	D	
SR	0.171157	0.150266	0.083338	0.113288
SH	0.040412	0.112878	0.264528	0.928142
TL	0.125123	0.200729	0.386463	0.143508

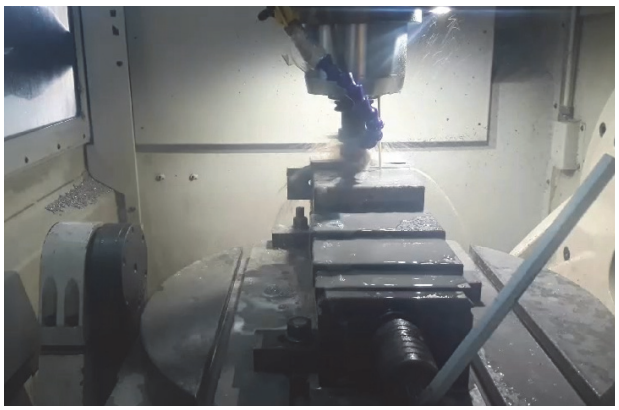

Figure 3 Experimental setting for the roller burnishing process

4 RESULTS AND DISCUSSIONS

4.1 ANOVA Analysis

Tab. 3 and Tab. 4 present experimental data and values of Kriging model parameters, respectively.

The ANOVA results of the *SR* are shown in Tab. 5. Significant parameters are single factors (*S*, *f*, and *D*) andquadratic factors (S^2 and f^2), as shown in Fig. 5a. The contributions of the *S*, *f*, and *D* are 20.21%, 23.43%, and 12.34%, respectively. The contributions of the S^2 and f^2 are 32.23% and 10.73%, respectively. The values of the R^2 value (0.9764), Adjusted R^2 (0.9683), and Predicted R^2 (0.9622) indicate that the *SR* model is adequate.

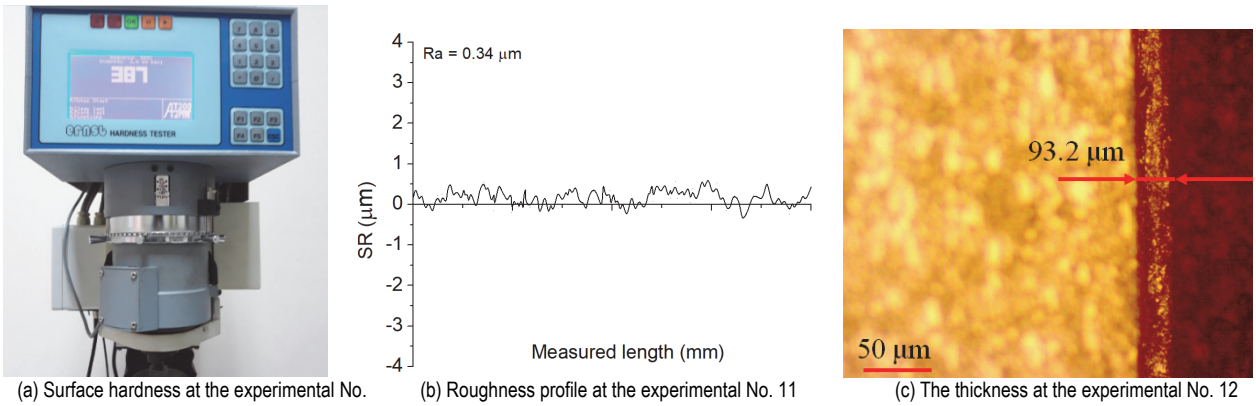

(a) Surface hardness at the experimental No. (b) Roughness profile at the experimental No. 11 (c) The thickness at the experimental No. 12

Figure 4 Example results of the multi-roller flat burnishing operation

The ANOVA results of the *SH* are shown in Tab. 6. Significant parameters are single factors (*S*, *f*, and *D*), interactive factors (*SD*, *SD*, and *fD*), and quadratic factors (S^2, f^2, and D^2), as shown in Fig. 5b. The contributions of the *S*, *f*, and *D* are 23.01%, 24.21%, and 21.65%, respectively. The contributions of the *SD*, *SD*, and *fD* are 3.06%, 5.03%, and 2.38%, respectively. The contributions of the S^2, f^2, and D^2 are 5.24%, 7.26%, and 8.16% respectively. The values of the R^2 value (0.9824), the Adjusted R^2 (0.9762), and the Predicted R^2 (0.9682) indicate that the *SH* model is adequate.

The ANOVA results of the *TL* are shown in Tab. 7. Significant parameters are single factors (*S*, *f*, and *D*), the interactive factor (*Sf*), and quadratic factors (S^2, f^2, and D^2), as shown in Fig. 5c. The contributions of the *S*, *f*, and *D* are 24.73%, 17.44%, and 26.51%, respectively. The contribution of the *Sf* is 2.96%. The contributions of the f^2, and D^{22} are 9.86%, 10.1%, and 7.37%, respectively. The values of the R^2 value (0.776), the Adjusted R^2 (0.9642), and the Predicted R^2 (0.9571) indicate that the *TL* model is adequate.

Table 5 Computed ANOVA results for the *SR*

So.	*SS*	*MS*	*F* Value	*p*-value
Model	0.10838	0.01204	24.92864	< 0.0001
S	0.51168	0.51168	1066.00777	< 0.0001
f	2.37274	2.37274	4943.21746	< 0.0001
D	2.14173	2.14173	4461.93969	< 0.0001
S^2	4.18739	4.18739	8723.72181	< 0.0001
f^2	1.39580	1.39580	2907.90727	< 0.0001
Residual	0.00242	0.00048		
Cor Total	0.11080			
R^2 = 0.9764; Adjusted. R^2 = 0.9683; Pred. R^2 = 0.9622				

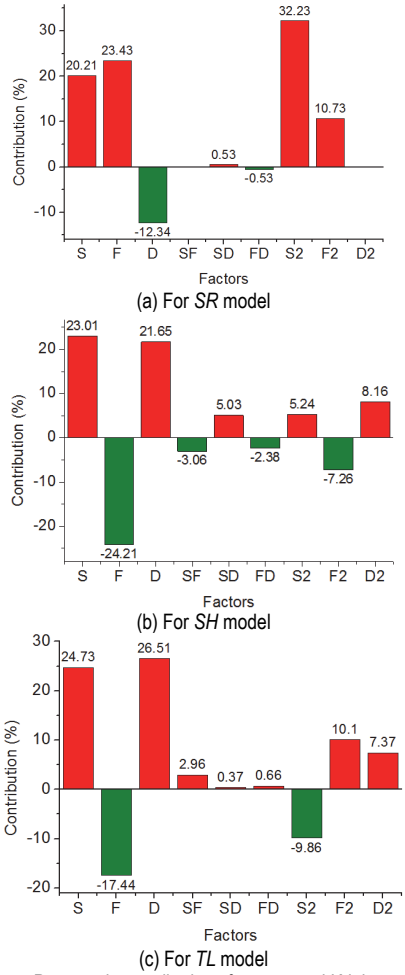

Figure 5 Parametric contributions for proposed Kriging models

Table 6 Computed ANOVA results for the *SH*

So.	*SS*	*MS*	*F* Value	*p*-value
Model	47962.7190	5329.19101	29.31302	0.0001
S	20192.3783	20192.3783	111.0674	< 0.0001
f	19709.1594	19709.5949	108.4095	< 0.0001
D	21477.5347	21477.5347	118.1364	< 0.0001
Sf	3166.62552	3166.62552	17.4179	0.0036
SD	6950.12614	6950.12614	38.2289	< 0.0001
fD	3331.12555	3331.12555	18.3227	0.0038
S^2	5407.93839	5407.93839	29.7461	< 0.0001
f^2	7525.87624	7525.87624	41.3958	< 0.0001
D^2	15051.7524	15051.7524	82.7916	< 0.0001
Residual	909.01424	181.80285		
Cor Total	48871.73333			
R^2 = 0.9824; Adjusted. R^2 = 0.9762; Pred. R^2 = 0.9682				

Table 7 Computed ANOVA results for the *TL*

So.	*SS*	*MS*	*F* Value	*p*-value
Model	13066.2688	1451.80765	25.40498	< 0.0001
S	21468.2608	21468.2608	375.6701	< 0.0001
f	15139.7682	15139.7682	264.9287	< 0.0001
D	23013.4894	23013.4894	402.7099	< 0.0001
S^2	8559.52495	8559.5249	149.7819	0.0015
f^2	8767.87038	8767.8703	153.4277	0.0014
D^2	6397.94106	6397.9410	111.9566	0.0054
Residual	285.73284	57.14657		
Cor Total	13352.00169			
R^2 = 0.9776; Adjusted. R^2 = 0.9642; Pred. R^2 = 0.9571				

4.2 Parametric Influences

As shown in Fig. 6a, when the *S* increases from 500 to 900 rpm, the *SR* is decreased by 26.6%. A further *S* increases the *SR* by around 51.1%. A higher *S* increases the machining frequency, leading to a higher temperature at the burnishing region. The hardness and strength of the workpiece surface consequently decrease. The material is easily burnished, resulting in a decrease in the peak and a filling of the valley; hence, the *SR* decreases. Alow *S* causes a stable burnishing operation; hence, a low *SR* is obtained. A higher *S* may cause excessive burnishing temperature, leading to work-hardening behavior. The hardness and strength of the workpiece surface consequently increase. The material is hardly compressed; hence, the *SR* increases. Moreover, excessive speed may cause vibration, leading to an unstable machining process; hence, the *SR* increases. A similar impact of the *S* on the *SR* can be found in the works of [5, 6, 12, 13].

As shown in Fig. 6b, when the *f* increases from 150 to 550 mm/min, the *SR* is increased by 50.2%. A low *f* decreases the distance between successive paths, leading to a higher machining frequency. Higher temperature is produced at the interfaces; hence, the hardness and strength of the workpiece surface consequently decrease. The material is softly compressed; hence, the *SR* decreases. Practically, a low *f* increases the burnishing time to process material. The material is thoroughly burnished due to the greater impact of the burnishing tool and regular metal flow; hence, the *SR* decreases. An increased *f* causes a larger distance between successive traces, leading to a lower machining frequency. The temperature slightly increases at the interfaces; hence, the hardness and strength of the workpiece surface slightly decrease. The material is hardly compressed; hence, the *SR* increases. A higher *f* reduces the burnishing time; hence, the impact of the burnishing tool decreases, resulting in a higher *SR*. A higher *SR* with an increased f can be found in the works of [5, 6, 12, 13].

As shown in Fig. 6c, when the *D* increases from 0.06 to 0.12 mm, the *SR* is decreased by 32.2%. A higher *D* increases the friction at the interfaces, leading to a higher machining temperature. The hardness and strength of the workpiece surface consequently decrease. The material is softly decreased and the *SR* decreases. An increased *D* causes higher machining pressure at the interfaces and the material is comprehensively compressed. The peaks are flatted and the valleys are filled; hence, the *SR* decreases. A higher *SR* with an increased *D* can be found in the works of [5, 6, 12, 13].

As shown in Fig. 7a, when the *S* increases from 500 to 1300 rpm, the *SH* increases by around 34.5%. A higher *S* increases the engagement frequency, leading to more burnishing traces on the machined surface. A higher degree of plastic deformation is obtained, resulting in work-hardening; hence, the *SH* decreases. Additionally, a higher *S* causes excessive machining temperature at the interfaces, resulting in work-hardening on the workpiece surface; hence, a higher *SH* is obtained. A similar impact of the tool's rotational speed on the surface hardness can be found in the works of [5-7].

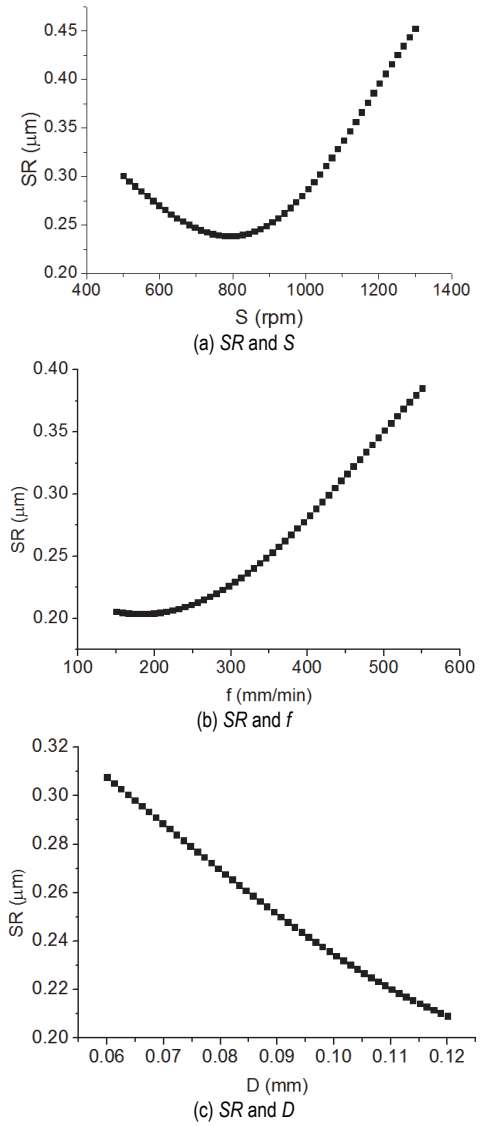

Figure 6 The impacts of process parameters on the *SR*

As shown in Fig. 7b, when the *f* increases from 150 to 550 mm/min, the *SH* decreases by around 29.2%. At a low *f*, the number of burnishing traces increases, and plastic deformation is more rigorous, leading to higher *SH*. A low *f* increases the machining temperature at the interfaces, leading to work-hardening; hence, a higher *SH* is obtained. A higher *f* causes a low degree of plastic deformation due to a higher distance among the consecutive traces; hence, the *SH* decreases. Additionally, a higher *f* reduces the burnishing time to compress material; hence, the impact of the burnishing tool decreases, resulting in a lower *SH*. A lower *SH* with an increased *f* can be found in the works of [5-7].

As shown in Fig. 7c, when the *D* increases from 0.06 mm to 0.12 mm, the *SH* increases by around 26.5%. A low *D* decreases the *SH* because of insufficient pressure, resulting in incomplete deformation action. A higher *D* increases the machining pressure; hence, the material is softly compressed and a higher *SH* is obtained. A higher *D* increases the machining temperature, leading to work-hardening behavior on the workpiece surface; hence, the SH increases. A higher *SH* with an increased *D* can be found in the works of [5-7].

Table 8 Testing results for developed Kriging models

No.	*SR*			*SH*			*TL*		
	Exp.	Krig.	ER / %	Exp.	Krig.	ER / %	Exp.	Krig.	ER / %
18	0.29	0.28	3.45	356	358	−0.56	69.8	68.4	2.01
19	0.32	0.31	3.13	338	336	0.59	82.8	82.4	0.48
20	0.27	0.26	3.85	393	391	0.51	104.7	103.8	0.86
21	0.35	0.34	2.94	477	475	0.42	125.4	124.2	0.96
22	0.28	0.27	3.70	393	394	−0.25	97.1	97.8	−0.72
23	0.31	0.3	3.33	408	410	−0.49	101.3	102.4	−1.09
24	0.18	0.19	−5.56	470	471	−0.21	130.6	131.5	−0.69

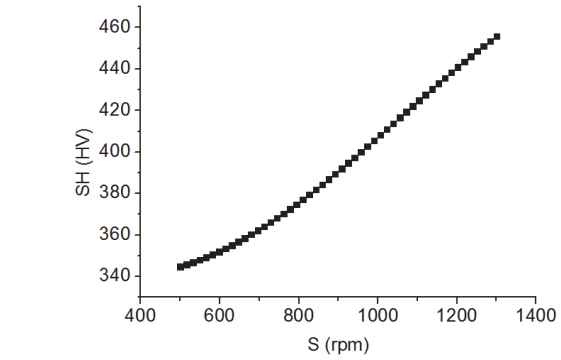

(a) *SH* and *S*

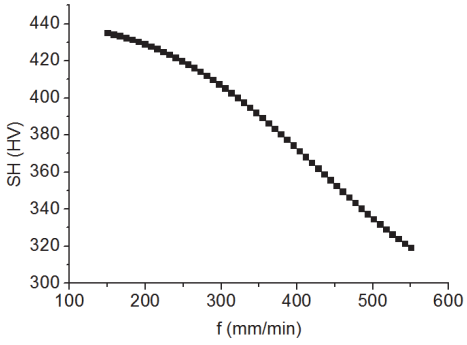

(b) *SH* and *f*

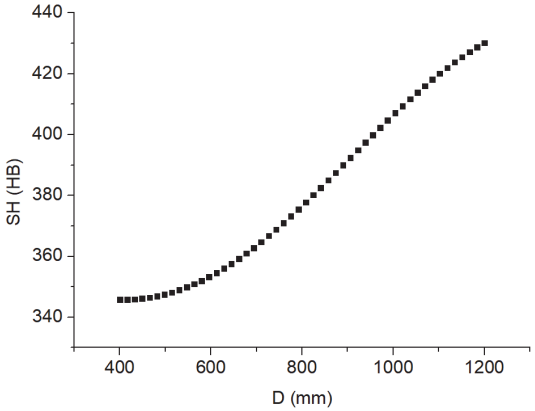

(c) *SH* and *D*

Figure 7 The impacts of process parameters on the *SH*

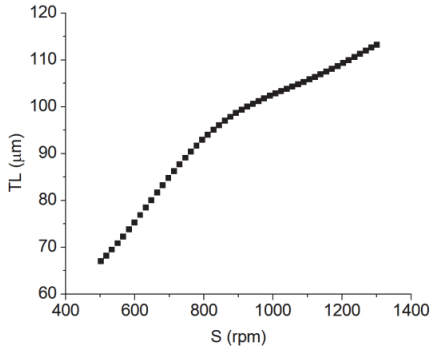

(a) *TL* and *S*

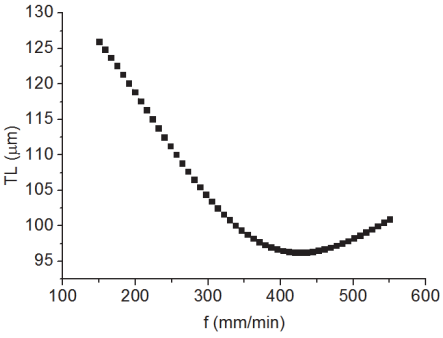

(b) *TL* and *f*

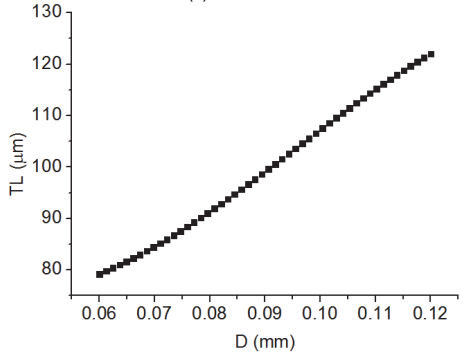

(c) *TL* and *D*

Figure 8 The impacts of process parameters on the *TL*

As shown in Fig. 8a, when the *S* increases from 500 to 1300 rpm, the *TL* increases by around 76.9%. A higher *S* causes burnishing engagement and a higher number of

burnishing traces are executed to process material. A higher degree of plastic deformation is obtained, leading to a higher *TL*. Additionally, a higher *S* increases the machining temperature at the interfaces, resulting in work-hardening behavior; hence, a higher *TL* is obtained. A higher *TL* with an increased *S* can be found in the work of [10].

As shown in Fig. 8b, when the *f* increases from 150 to 550 mm/min, the *TL* decreases by around 21.3%. A low *f* increases the machining frequency, leading to a higher burnishing temperature. The work-hardening behavior is produced; hence, a higher *TL* is obtained. A higher *f* decreases the number of burnishing traces, leading to a low degree of plastic deformation; hence, the *TL* decreases. A lower *SH* with an increased *f* can be found in the work of [10].

As shown in Fig. 8c, when the *D* increases from 0.04 mm to 0.12 mm, the *TL* increases by around 56.3%). A low *D* causes low plastic deformation of the workpiece surface; hence, the *TL* decreases. A higher *D* increases the machining pressure, resulting in a high degree of plastic deformation. More material is softly burnished and the *TL* increases. Additionally, a higher *D* increases the machining temperature, leading to work-hardening behavior; hence, a higher *TL* is obtained. A similar impact of the *D* on the *TL* can be found in the work of [10].

4.3 Optimizing Outcomes Generated by the CSA

The weights of the *SR*, *SH*, and *TL* produced by the CRITIC method are 0.34, 0.33, and 0.33, respectively (Tab. 8). The 3D graph produced by the CSA is shown in Fig. 9. The population size, the maximum number of iterations, the flight radius, and the perceptual probability were 100, 100, 1, and 0.1, respectively. The optimal data of the *S*, *f*, and *D* were 912 rpm, 150 mm/min, and 0.12 mm, respectively (Tab. 9). The *SR* was decreased by 33.3%, while the *SH* and *TL* are improved by 26.9% and 48.6%, respectively at the optimal solution.

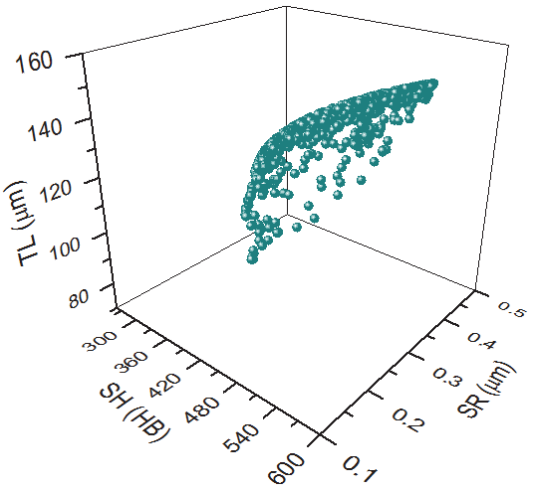

Figure 9 3D Graph produced by the CSA

4.4 Scientific and Industrial Contributions

In this investigation, the *SR*, *SH*, and *TL* of a multi-roller flat burnishing process were enhanced using optimum factors. The academic remarks are expressed as:

The optimization approach using the Kriging model-CRITIC-CSA can be effectively utilized to determine optimal outcomes of the burnishing processes and other machining operations.

The developed Kriging models can be applied to describe the complex data of the burnishing and machining processes.

The Pareto fronts presenting the global references among burnishing responses can be applied to select optimal data of the *S*, *D*, *f*, *SR*, *SH*, and *TL*.

The industrial values are expressed as:

The impacts of process parameters on the burnishing responses can help the operators deeply understand the physical insights of the burnishing operation.

The developed Kriging models of the *SR*, *SH*, and *TL* can be precisely utilized to calculate the machining targets for different deployments.

The optimal data can be applied to the practical burnishing operation to boost the performance measures.

Table 9 The computed weights of the burnishing responses

Responses	I_j	C_j	ω_i
SR	1.25680	0.3363	0.34
SH	1.12630	0.3228	0.33
TL	1.15680	0.3290	0.33

Table 10 Optimization results generated by the CSA

Method	parameters			Responses		
	S	*f*	*D*	*SR*	*SH*	*TL*
Common values	900	350	0.09	0.27	391	98.5
Optimal values	912	150	0.12	0.18	496	146.4
Improvement (%)				−33.3	26.9	48.6

The multi-roller flat burnishing process can be effectively applied to enhance the surface properties and production rate for different flat surfaces.

5 CONCLUSIONS

In this investigation, process parameters of the multi-roller flat burnishing process were optimized to improve the *SH* as well as *TL* and decrease the *SR*. The parameter inputs were the *S*, *f*, and *D*. The Kriging models and CSA were applied to find optimal outcomes. The obtained conclusions can be expressed as:

1. To reduce roughness, the highest depth was applied, while low values of the feed and speed were recommended. To increase the hardness and thickness, higher values of the speed and depth were employed, while a low feed was utilized.

2. For the *SR*, the *f* has the highest contribution, followed by the *D*, and *S*, respectively. For the *SH*, the *D* was named as the most effective factor, followed by the *S* and *f*, respectively. For the *TL*, the *D* has the highest contribution, followed by the *S* and *f*, respectively.

3. The optimal outcomes of the *S*, *f*, and *D* were 912 rpm, 150 mm/min, and 0.12 mm, respectively. The *SH* and *TL* were improved by 26.9% and 48.6%, respectively. while the *SR* was decreased by 33.3%,

4. This study did not address the impacts of the configuration of the burnishing tool and environmental as well as economic metrics. The machining costs, energy consumption, and roller characteristics (coatings, shapes, and dimensions) will be considered in future works.

6 REFERENCES

[1] Basak, H. & Haldun Goktas, H. (2009). Burnishing process on al-alloy and optimization of surface roughness and surface hardness by fuzzy logic. *Materials & Design*, *30*(4), 1275-1281. https://doi.org/10.1016/j.matdes.2008.06.063

[2] Stanković, I., Perinić, M., Jurković, Z., Mandić, V. & Maričić, S. (2012). Usage of neural network for the prediction of surface roughness after the roller burnishing. *Metalurgija*, *51*(2), 207-210.

[3] Revankar, G. D., Shetty, R., Rao, S. S., & Gaitonde, V. N. (2014). Selection of optimal process parameters in ball burnishing of titanium alloy. *Machining Science and Technology*, *18*(3), 464-483. https://doi.org/10.1080/10910344.2014.897848

[4] Vukelic, D., Tadic, B., Dzunic, D., Kocovic, V., Brzakovic, L., Zivkovic, M., & Simunovic, G. (2017). Analysis of ball-burnishing impact on barrier properties of wood workpieces. *International Journal of Advanced Manufacturing Technology*, *92*, 129-138. https://doi.org/10.1007/s00170-017-0134-3

[5] Stalin John, M. R., Banerjee, N., Shrivastava, K., & Vinayagam, B. K. (2017). Optimization of roller burnishing process on EN-9 grade alloy steel using response surface methodology. *Journal of the Brazilian Society of Mechanical Sciences and Engineering*, *39*, 3089-3101. https://doi.org/10.1007/s40430-016-0674-8

[6] Patel, K. A. & Brahmbhatt, P. K. (2018). Response surface methodology based desirability approach for optimization of roller burnishing process parameter. *Journal of The Institution of Engineers (India): Series C*, *99*, 729-736. https://doi.org/10.1007/s40032-017-0368-8

[7] Stalin John, M. R., Balaji, B., & Vinayagam, B. K. (2017). Optimisation of internal roller burnishing process in CNC machining center using response surface methodology. *Journal of the Brazilian Society of Mechanical Sciences and Engineering*, *39*, 4045-4057. https://doi.org/10.1007/s40430-017-0871-0

[8] Yuan, X. L., Sun, Y. W., Gao, L. S., & Jiang, S. L. (2016). Effect of roller burnishing process parameters on the surface roughness and microhardness for TA2 alloy. *International Journal of Advanced Manufacturing Technology*, *85*, 1373-1383. https://doi.org/10.1007/s00170-015-8031-0

[9] Shankar, E., Balasivanandha Prabu, S., Sampath Kumar, T., & Stalin John, M. R. (2018). Investigation of TiAlN coated roller burnishing on Al-(B4C)p MMC workpiece material. *Materials and Manufacturing Processes*, *33*(11), 1242-1249. https://doi.org/10.1080/10426914.2018.1453160

[10] Nguyen, T. T. & Le, X. B. (2018). Optimization of interior roller burnishing process for improving surface quality. *Materials and Manufacturing Processes*, *33*(11), 1233-1241. https://doi.org/10.1080/10426914.2018.1453159

[11] Cagan, S. C., Aci, M., Buldum, B. B., & Aci, C. (2019). Artificial neural networks in mechanical surface enhancement technique for the prediction of surface roughness and microhardness of magnesium alloy. *Bulletin of the Polish Academy of Sciences: Technical Sciences*, *67*(4), 729-739.

[12] Nguyen, T. T. (2021). Multi-response performance optimization of burnishing operation for improving hole quality. *Journal of the Brazilian Society of Mechanical Sciences and* Engineering, *43*, 560. https://doi.org/10.1007/s40430-021-03274-0

[13] Nguyen, T. T. & Le, M. T. (2021). Optimization of internal burnishing operation for energy efficiency, machined quality, and noise emission. *International Journal of Advanced Manufacturing Technology*, *114*, 2115-2139. https://doi.org/10.1007/s00170-021-06920-y

[14] Nguyen, T. T., Nguyen, T. A., Trinh, Q. H., Le, X. B., Pham, L. H., & Le, X. H. (2022). Artificial neural network-based optimization of operating parameters for minimum quantity lubrication-assisted burnishing process in terms of surface characteristics. *Neural Computing and Applications*, *34*, 7005-7031. https://doi.org/10.1007/s00521-021-06834-6

[15] Nguyen, T. T., Nguyen, T. A., Trinh, Q. H., & Le, X. B. (2022). Multi-performance optimization of multi-roller burnishing process in sustainable lubrication condition. *Materials and Manufacturing Processes*, *37*(4), 407-427. https://doi.org/10.1080/10426914.2021.1962533

[16] Prasad, K. A. & John, M. R. S. (2021). Optimization of external roller burnishing process on magnesium silicon carbide metal matrix composite using response surface methodology. *Journal of the Brazilian Society of Mechanical Sciences and Engineering*, *43*, 342. https://doi.org/10.1007/s40430-021-03069-3

[17] Van, A. & Nguyen, T. (2022). Investigation and optimization of MQL system parameters in the roller-burnishing process of hardened steel. *Strojniškivestnik Journal of Mechanical Engineering*, *68*(3), 155-165. https://doi.org/10.5545/sv-jme.2021.7473

[18] Varga, G. & Ferencsik, V. (2022). Investigation of the effect of surface burnishing on stress condition and hardening phenomena. *Tehnički vjesnik*, *29*(4), 1247-1253. https://doi.org/10.17559/TV-20211110171854

[19] Van, A. & Nguyen, T. (2023). Multi-response optimization of burnishing variables for minimizing environmental impacts. *Tehnički vjesnik*, *30*(1), 169-177. https://doi.org/10.17559/TV-20220709090615

[20] Tadic, B., Randjelovic, S., Todorovic, P., Zivkovic, J., Kocovic, V., Budak, I., & Vukelic, D. (2016). Using a high-stiffness burnishing tool for increased dimensional and geometrical accuracies of openings. *Precision Engineering*. *43*, 335-344. https://doi.org/10.1016/j.precisioneng.2015.08.014

[21] Randjelovic, S., Tadic, B. Todorovic, P. M., Danijela, M., Radenkovic, M., & Tsiafis, C. (2015). Modelling of the ball burnishing process with a high-stiffness tool. *International Journal of Advanced Manufacturing Technology*, *81*, 1509-1518. https://doi.org/10.1007/s00170-015-7319-4

[22] Tadic, B. Todorovic, P. M., Luzanin, O., Miljanic, D., Jeremic, B. M., Bogdanovic, B., & Vukelic, D. (2013). Using specially designed high-stiffness burnishing tool to achieve high-quality surface finish. *International Journal of Advanced Manufacturing Technology*, *67*(1-4), 601-611. https://doi.org/10.1007/s00170-012-4508-2

[23] Jerez-Mesa, R., Travieso-Rodriguez, J. A., Gomez-Gras, G., & Lluma-Fuentes, J. (2018). Development, characterization and test of an ultrasonic vibration-assisted ball burnishing tool. *Journal of Materials Processing Technology*, *257*, 203-212. https://doi.org/10.1016/j.jmatprotec.2018.02.036

[24] Kanovic, Z., Vukelic, D., Simunovic, K., Prica, M., Saric, T., Tadic, B., & Simunovic, G. (2022). The modelling of surface roughness after the ball burnishing process with a high-stiffness tool by using regression analysis, artificial neural networks, and support vector regression. *Metals*, *12*, 320. https://doi.org/10.3390/met12020320

[25] Douglas, C. M. (2012). *Design and Analysis of Experiments*. Wiley.

[26] Vukelic, D., Simunovic, K., Kanovic, Z., Saric, T., Tadic, B., & Simunovic, G. (2021). Multi-objective optimization of steel AISI 1040 dry turning using genetic algorithm. *Neural Computing and Applications*, *33*, 12445-12475. https://doi.org/10.1007/s00521-021-05877-z

Contact information:

An-Le VAN
Faculty of Engineering and Technology, Nguyen Tat Thanh University,
300A Nguyen Tat Thanh Street, Ward 13, District 4,
Ho Chi Minh City 70000, Vietnam
E-mail: lvan@ntt.edu.vn

Xuan-Ba DANG
(Corresponding author)
Department of Automatic Control, Ho Chi Minh City University of Technology
and Education, No. 1 Vo Van Ngan Street, Linh Chieu Ward, Thu Duc City,
Ho Chi Minh City 70000, Vietnam
E-mail: badx@hcmute.edu.vn

Trung-Thanh NGUYEN
Faculty of Mechanical Engineering, Le Quy Don Technical University,
236 Hoang Quoc Viet, Ha Noi 100000, Vietnam
E-mail: trungthanhnguyen@lqdtu.edu.vn